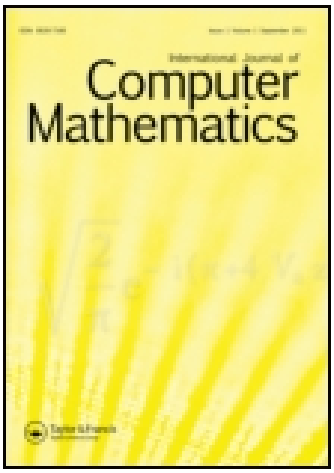

International Journal of Computer Mathematics

Publication details, including instructions for authors and subscription information:
http://www.tandfonline.com/loi/gcom20

Hexagonal grid methods with applications to partial differential equations

D. Lee[a], H.C. Tien[b], C.P. Luo[b] & H.-N. Luk[c]

[a] Department of Applied Mathematics, Tunghai University, Taichung, Taiwan

[b] Department of Financial and Computational Mathematics, Providence University, Taichung, Taiwan

[c] Department of Anesthesia, China Medical University Beigang Hospital, Taichung, Taiwan

Accepted author version posted online: 14 Nov 2013.Published online: 26 Mar 2014.

To cite this article: D. Lee, H.C. Tien, C.P. Luo & H.-N. Luk (2014) Hexagonal grid methods with applications to partial differential equations, International Journal of Computer Mathematics, 91:9, 1986-2009, DOI: 10.1080/00207160.2013.864392

To link to this article: http://dx.doi.org/10.1080/00207160.2013.864392

International Journal of Computer Mathematics, 2014
Vol. 91, No. 9, 1986–2009, http://dx.doi.org/10.1080/00207160.2013.864392

Hexagonal grid methods with applications to partial differential equations

D. Lee[a*], H.C. Tien[b], C.P. Luo[b] and H.-N. Luk[c]

[a]*Department of Applied Mathematics, Tunghai University, Taichung,Taiwan;* [b]*Department of Financial and Computational Mathematics, Providence University, Taichung, Taiwan;* [c]*Department of Anesthesia, China Medical University Beigang Hospital, Taichung, Taiwan*

(*Received 2 April 2013; revised version received 29 July 2013; second revision received 3 September 2013; accepted 3 November 2013*)

We consider in this work hexagonal grids for two-dimensional applications. A finite volume-based finite difference approach to solving Laplacian-related differential equations on hexagonal grids is developed. Both ordinary and compact hexagonal seven-point schemes are investigated. Theoretical properties of the associated linear algebraic systems are determined. These methods are applied to solve PDEs on both regular and curved domains, successfully exhibiting linear and spiral wave propagations in regular domains and curved wave in a reversed C-type domain.

Keywords: compact scheme; hexagonal finite volume; finite difference; monodomain model; reaction-diffusion

2010 AMS Subject Classifications: 65M06; 65M08

1. Introduction

Hexagonal finite volumes (FVs) is of interest in a recent study of the electrophysiology of human heart [13], which explored the origin of *U*-wave in electrocardiogram (ECG) and adopted hexagonal subdomains in their computations. However, it was a pure algebraic approach in obtaining the ECG without coupling diffusion. Actually, heart electrical activity can be described by a system of reaction-diffusion (R-D) equations. Computer modelling has become a powerful tool and numerical simulation can provide detailed observations for electrical activities of the heart. It is a useful tool for understanding the mechanism of heart rhythm dynamics. We refer to [4] for general references.

We consider in this work hexagonal grids for two-dimensional applications, and investigate FV-based finite difference (FD) technique in solving differential equations. Both ordinary second-order and compact fourth-order seven-point methods are developed and analysed, with applications to Poisson equation and R-D systems. A construction algorithm is described for practical applications. With such, the proposed method can be easily implemented on regular and irregular computational domains. In addition to solving several test problems with known

*Corresponding author. Email: danlee@thu.edu.tw

solutions and justifying the methods accordingly, we solve the monodomain model and simulate electrical wave propagation on a two-dimensional cardiac tissue. Linear wave propagation is observed on both regular and irregular geometric domains, while spiral wave propagation is observed on an approximated square domain.

Note that the left ventricle of the heart can be approximated by an ellipsoid of revolution (see Figure 2 in [7]) and hexagonal FVs are relatively easy to construct for such domains. We can apply the hexagonal finite volume method (FVM) to an electrophysiological simulation of the cardiac tissue on the horizontal cross-section or the apex to the base longitudinal section of the left ventricle of the heart. This will simplify the geometric modelling and direct numerical simulation yielding a significant reduction in computational costs.

As for the remaining sections, the notations and terminologies of regular hexagons are introduced in Section 2. For regular hexagons in general positions, a FV approach to solving the Poisson equation is discussed in Section 2.1. This suggests in Section 2.2 an ordinary seven-point scheme for discretisation of the two-dimensional Laplacian. Furthermore, a fourth-order hexagonal compact seven-point scheme is derived. Application of general conforming hexagonal FVs are made easy with a construction algorithm, which we proposed in Section 2.3. Applications to solving differential equations are described in Section 3, in which four variations of seven-point schemes are analysed for evolution equations. Numerical experiments and observations are discussed in Section 4, and conclusions drawn in the final section. Some rigorous arguments involving trigonometric identities and a lower bound estimate of the seven-point Laplacian are presented respectively in Appendices 1 and 2.

2. Hexagonal grid method

For two-dimensional applications of configurations consisting of cartesian type (regular) hexagons, we denote by r the radius (also edge length) of hexagons and $h = (\sqrt{3}/2)r$ half of the *centre-to-centre* distance. Relevant numerics of the coordinates of centres and vertices are given in Tables 1 and 2, based on two configurations with one indicated in Figure 1(a). The area of a hexagon is $|\Omega| = (3\sqrt{3}/2)r^2 = 2\sqrt{3}h^2$.

For a hexagon in general configuration with phase angle φ, we consider the centre $P_0 = (x_0, y_0)$ and its six neighbours (Figure 1(b)),

$$P_j = (x_j, y_j) = (x_0, y_0) + 2h(\cos\theta_j, \sin\theta_j), \quad \theta_j = \varphi + \frac{\pi}{6} + \frac{j\pi}{3}, \quad j = 1, \ldots, 6.$$

Table 1. Hexagon in configuration type I.

Phase angle: $\boldsymbol{\varphi} = \mathbf{0}$		
Centre point	i^{even}	i^{odd}
$cx(i,j)$	$(1.5i - 0.5)r$	
$cy(i,j)$	$2jh$	$(2j-1)h$
Vertices	$V_k = (vx(i,j,k), vy(i,j,k)),\ k = 1, 2, \ldots, 6$	
$vx(i,j,k)$	$cx(i,j) + r\cos\left(\varphi + \frac{k\pi}{3}\right),\ k = 1, 2, \ldots, 6$	
$vy(i,j,k)$	$cy(i,j) + r\sin\left(\varphi + \frac{k\pi}{3}\right),\ k = 1, 2, \ldots, 6$	
Neighbour centres	$P_k = V_k + V_{k+1} - P_0,\ k = 1, 2, \ldots, 6$	

Table 2. Hexagon in configuration type II.

Phase angle: $\varphi = -\frac{\pi}{6}$		
Centre point	j^{even}	j^{odd}
$cx(i,j)$	$2ih$	$(2i-1)h$
$cy(i,j)$	$(1.5j-0.5)r$	
Vertices	$V_k = (vx(i,j,k), vy(i,j,k)),\ k = 1,2,\ldots,6$	
$vx(i,j,k)$	$cx(i,j) + r\cos\left(\varphi + \frac{k\pi}{3}\right),\ k = 1,2,\ldots,6$	
$vy(i,j,k)$	$cy(i,j) + r\sin\left(\varphi + \frac{k\pi}{3}\right),\ k = 1,2,\ldots,6$	
Neighbour centres	$P_k = V_k + V_{k+1} - P_0,\ k = 1,2,\ldots,6$	

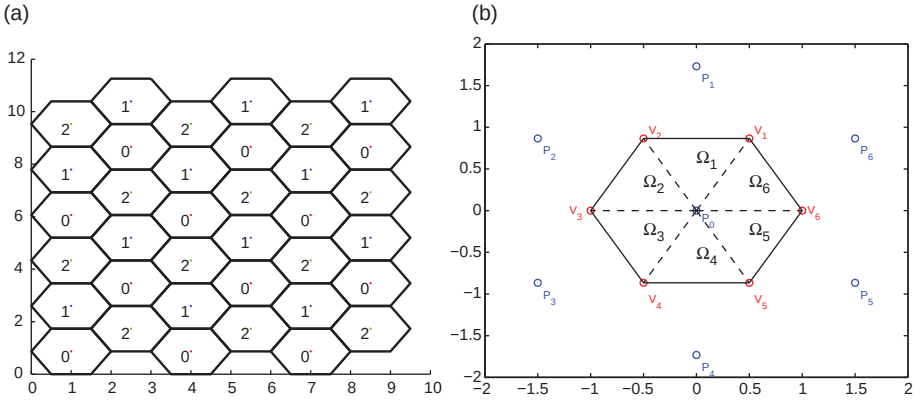

Figure 1. Type I hexagonal FVs and neighbourhood, phase angle $\varphi = 0$. (a) Net of hexagons, in three-colour ordering, (b) Neighbourhood.

2.1 *Hexagonal FV approach*

In application of FVM [21], a differential equation is solved in an averaged form. We consider Poisson equation and its integral formulation

$$\nabla(k\nabla u) = f, \quad \frac{1}{|\Omega|}\iint_\Omega \operatorname{div}(k\nabla u)\,\mathrm{d}x\,\mathrm{d}y = \frac{1}{|\Omega|}\iint_\Omega f\,\mathrm{d}x\,\mathrm{d}y.$$

The domain integral of the divergence yields a boundary integral of the *normal flux*, which is then reduced to a discrete approximation. The specialisation to a hexagonal FV with unit constant diffusivity ($k = 1$), reads

$$\begin{aligned}\frac{1}{|\Omega|}\iint_\Omega \operatorname{div}(k\nabla u)\,\mathrm{d}x\,\mathrm{d}y &= \frac{1}{|\Omega|}\int_{\partial\Omega} k\frac{\partial u}{\partial \overrightarrow{n}}\,\mathrm{d}\gamma(t) \approx \frac{1}{|\Omega|}\sum_{i=1}^{6}\left(k\frac{\partial u}{\partial \overrightarrow{n}}(m_i)\right)|\Delta\gamma_i| \\ &\approx \frac{1}{2\sqrt{3}h^2}\sum_{i=1}^{6}\frac{u(P_i)-u(P_0)}{\sqrt{3}r}r = \frac{1}{h^2}\frac{1}{6}\sum_{i=1}^{6}(u(P_i)-u(P_0)),\end{aligned}$$

where $|\Delta\gamma_i|$ denotes the length of the ith boundary edge and m_i the mid-point of that edge. The boundary integral is thus approximated by a discrete seven-point stencil. It turns out a surprise that the mid-point rule, seemingly just a (local) second-order approximation to each line integral,

achieves the same order of global accuracy for the whole boundary (and domain) integral. We discuss and prove this from a different perspective next.

2.2 *Hexagonal FD approach*

Consider Poisson equation in the simplest form, $\triangle u = u_{xx} + u_{yy} = f(x, y)$.

THEOREM 2.1 (Second-order hexagonal ordinary seven-point (*H7*) scheme) *The differential relation* $u_{xx}(x_0, y_0) + u_{yy}(x_0, y_0) = f(x_0, y_0)$ *is approximated by the discrete hexagonal ordinary seven-point scheme*

$$\frac{1}{h^2}\left(-u(x_0, y_0) + \frac{1}{6}\sum_{j=1}^{6} u(x_j, y_j)\right) = f(x_0, y_0), \tag{1}$$

which is second-order accurate, that is,

$$u_{xx} + u_{yy} = \frac{1}{h^2}\left(\frac{1}{6}\sum_{i=1}^{6} u(P_i) - u(P_0)\right) - \frac{h^2}{4}(u_{xxxx} + 2u_{xxyy} + u_{yyyy}) + \mathcal{O}(h^4) \tag{2}$$

$$= \frac{1}{h^2}\left(\frac{1}{6}\sum_{i=1}^{6} u(P_i) - u(P_0)\right) + \mathcal{O}(h^2). \tag{3}$$

Proof For sufficiently smooth u, we obtain formally

$$\begin{aligned}\frac{1}{6}\sum_{j=1}^{6}(u(P_j) - u(P_0)) &= \frac{1}{6}\sum_{j=1}^{6}\sum_{1\le m+n}(2h)^{m+n}\frac{(\partial_x^m\partial_y^n u(P_0))}{m!n!}\cos^m\theta_j\sin^n\theta_j \\ &= \sum_{1\le m+n}\left((2h)^{m+n}\frac{(\partial_x^m\partial_y^n u(P_0))}{m!n!}\frac{1}{6}\sum_{j=1}^{6}\cos^m\theta_j\sin^n\theta_j\right) \\ &= \frac{(2h)^2}{4}(u_{xx} + u_{yy}) + \frac{(2h)^4}{64}(u_{xxxx} + 2u_{xxyy} + u_{yyyy}) + \mathcal{O}(h^6).\end{aligned}$$

Here we appeal to Lemmas A.2 and A.3 (with φ replaced by $\varphi + \pi/6$) in Appendix 1. Thus proves the Theorem. ■

Remark 1 The error analysis requires C^6- and C^4-*smoothness* of u for Equations (2) and (3), respectively. Making use of the estimate, we gain further by a bootstrapping strategy.

THEOREM 2.2 (Fourth-order hexagonal compact seven-point (*H7c*) scheme as deferred correction)

$$\frac{1}{h^2}\left(-u(P_0) + \frac{1}{6}\sum_{i=1}^{6} u(P_i)\right) = \frac{3}{4}f(P_0) + \frac{1}{24}\sum_{i=1}^{6} f(P_i) + \mathcal{O}(h^4). \tag{4}$$

Proof We proceed with Equation (2).

$$\begin{aligned} f(P_0) &= (u_{xx} + u_{yy})(P_0) \\ &= \frac{1}{h^2}\left(\frac{1}{6}\sum_{i=1}^{6} u(P_i) - u(P_0)\right) - \frac{h^2}{4}(f_{xx} + f_{yy})(P_0) + \mathcal{O}(h^4) \\ &= \frac{1}{h^2}\left(\frac{1}{6}\sum_{i=1}^{6} u(P_i) - u(P_0)\right) - \frac{h^2}{4}\left(\frac{1}{h^2}\left(\frac{1}{6}\sum_{i=1}^{6} f(P_i) - f(P_0)\right) + \mathcal{O}(h^2)\right) + \mathcal{O}(h^4) \\ &= \frac{1}{h^2}\left(\frac{1}{6}\sum_{i=1}^{6} u(P_i) - u(P_0)\right) + \frac{1}{4}f(P_0) - \frac{1}{24}\sum_{i=1}^{6} f(P_i) + \mathcal{O}(h^4). \end{aligned}$$

The assertion follows after rearrangement. ■

Remark 2 The special case of type II hexagons, embedded in a mesh consisting of equilateral triangles, was discussed in [9]. Equation (2) in this cited reference is almost identical to the *H7c* scheme we proposed, and was used there to derive amazing fast Fourier transform methods in a direct method approach, which we believe may be extended to multi-block situations for parallel computations.

This implicit solution (Equation (4)) yields conveniently associated matrix properties which will be discussed in Section 3. We refer to [5,14] for compact schemes on rectangular grids. Comparisons among these hexagonal (and rectangular) FD schemes are discussed in Section 4.

2.3 *General (non-regular) conforming hexagonal FVs*

For general hexagonal FV applications, we propose a procedure for the construction of the discrete geometry and local topology. This is applicable to (and essential for) irregular domains approximated by hexagons. The algorithm applies to regular domains as well. We require only

Hypothesis 2.3 (Minimal assumptions for practical applications)

- The FVs are conforming, i.e. two neighbour cells share exactly two vertices (and the connecting edge).
- Input data consists of only a list of cell centres.

We state the following for general applications.

ALGORITHM 1 (Effective construction of general hexagonal FVs)

(1) *Construct the edges as to bisect the centre–centre connecting line segments. These edges are confined to the intersections with neighbour edges in the next step.*
(2) *Vertices are defined as the intersections of neighbour edges around each centre.*
(3) *In order to index vertices without repetitions, we run the scan a second time and eliminate repeated vertices.*

(4) *Set* (*Define*) *the neighbourhood topology and identify boundary cells.*
(5) *Re-number to separate interior and boundary cells, and generate a linear list* (*efficient*) *for later operations.*

To perform computation using hexagonal FVs in solving practical problems, more algorithms and (consistent) data structures can be designed as natural follow-up to this fundamental algorithm. All these algorithms extends obviously to quadrilateral FVs.

Remark 3 On a lattice of hexagons as shown in Figure 1(a), *three-colour* algorithm is applicable to (FV) centre nodes, and applies as well to irregular domains embedded in a cartesian mesh. It guides multi-block iterations in solving both static and transient problems. Further study will be published elsewhere because of limitation of space.

3. Computation of differential equations on hexagonal grids

Here we consider ordinary and compact seven-point schemes (*H7,H7c*) for solving two-dimensional Laplacian-related problems.

3.1 *Application in solving two-dimensional Poisson equation*

The hexagonal seven-point stencil consists of negative diagonal and positive weights off the diagonal. For a *Dirichlet* problem, this immediately implies that the discrete seven-point two-dimensional Laplacian on hexagonal FVs satisfies the discrete maximum principle, which in turn implies the stability of classical linear iterative methods such as *GS* or *SSOR*. We note the negation of the matrix is symmetric positive-definite and actually an *M-matrix*. Modern *conjugate gradient-like* iterative methods perform very well in sparse format. For a *Neumann* problem, the typical *rank-one projection* approach works well.

Aiming at applications mostly in non-cartesian type regions, we will use iterative methods exclusively. We refer to [3] for further details in relevant matrix theory, and [15] for iterative methods. Pickering's [9] work is recommended for fast method in production runs on rectangular domains.

3.2 *Application in solving time-dependent problems*

We consider a system of R-D equations

$$\begin{aligned} u_t &= D_1(u_{xx} + u_{yy}) + f(u, v), \\ v_t &= D_2(v_{xx} + v_{yy}) + g(u, v), \end{aligned} \tag{5}$$

with non-negative constant diffusivities. For simplicity, we describe algorithms for a single component,

$$u_t = D(u_{xx} + u_{yy}) + f(u, v),$$

with positive constant diffusivity. Proper initial and boundary conditions are assumed. In application of a two-level time-marching procedure with h_t denoting the temporal stepsize, we note the following.

Example 3.1 (Fourth-order fully implicit scheme)

$$\frac{3}{4}\frac{u_{P_0}^{n+1}-u_{P_0}^{n}}{h_t}+\frac{1}{24}\sum_{i=1}^{6}\frac{u_{P_i}^{n+1}-u_{P_i}^{n}}{h_t}=\frac{D}{h^2}\left(-u_{P_0}^{n+1}+\frac{1}{6}\sum_{i=1}^{6}u_{P_i}^{n+1}\right)+\frac{3}{4}f_{P_0}^{n+1}+\frac{1}{24}\sum_{i=1}^{6}f_{P_i}^{n+1},$$

or

$$\left(\frac{3}{4}+\frac{Dh_t}{h^2}\right)u_{P_0}^{n+1}+\left(\frac{1}{24}-\frac{Dh_t}{6h^2}\right)\sum_{i=1}^{6}u_{P_i}^{n+1}=\frac{3}{4}(u_{P_0}^{n}+h_t f_{P_0}^{n+1})+\frac{1}{24}\sum_{i=1}^{6}(u_{P_i}^{n}+h_t f_{P_i}^{n+1}).$$

In matrix form,

$$\begin{aligned}\left(\boldsymbol{Q}_1+\frac{Dh_t}{h^2}\boldsymbol{Q}_2\right)u^{n+1}&=\boldsymbol{Q}_1u^n+h_t\boldsymbol{Q}_1f^{n+1},\\ \boldsymbol{K}_4u^{n+1}&=u^n+h_tf^{n+1},\end{aligned}\tag{6}$$

with

$$\boldsymbol{Q}_1=\frac{3}{4}\boldsymbol{I}+\frac{1}{24}\boldsymbol{E},\quad \boldsymbol{Q}_2=\boldsymbol{I}-\frac{1}{6}\boldsymbol{E},\quad \text{and}\quad \boldsymbol{K}_4=\boldsymbol{I}+\frac{Dh_t}{h^2}\boldsymbol{Q}_1^{-1}\boldsymbol{Q}_2.$$

Here the *incidence matrix* $\boldsymbol{E}$, related to the neighbourhood topology of all the hexagon centres, may include or exclude ghost cells up to proper interpretation. To apply *successive substitutions* (SS), we consider

$$\begin{aligned}&u^{n+1,0}:=u^n,\\ &u^{n+1,k}:=\boldsymbol{\Phi}u^{n+1,k-1}:=\boldsymbol{K}_4^{-1}u^{n+1,k-1}+h_t\boldsymbol{K}_4^{-1}f(u^{n+1,k-1},v^{n+1,k-1}),\quad k=1,2,\dots.\end{aligned}\tag{7}$$

Our primary interest is in applications on irregular domains, we note only the following for linear stability.

(1) In the pure diffusion case ($f=0$), the discrete seven-point (negative) Laplacian ($\boldsymbol{Q}_2$) is an *M-matrix* as noted in the previous subsection, and $\boldsymbol{Q}_1$ an *averaging operator* with positive weights. All of these imply that $\boldsymbol{K}_4$ is an *M-matrix* and *inverse-positive*. It is easily seen that $\boldsymbol{K}_4$ is strictly diagonally dominant and $\|\boldsymbol{K}_4\|>1$, $\|\boldsymbol{K}_4^{-1}\|<1$. The scheme is unconditionally stable and preferable to the next semi-implicit one.

Actually, the square matrices $\boldsymbol{Q}_1,\boldsymbol{Q}_2$ and $\boldsymbol{E}$ share the same basis vectors. To be precise and prepare for future work, let

$$\sigma_m=\min \mathrm{Spec}_{Q_2},\quad \sigma_M=\max \mathrm{Spec}_{Q_2}.$$

Then, by Gershgorin circles,

$$0<\sigma_m\le \mathrm{Spec}_{Q_2}\le\sigma_M\le 2.\tag{8}$$

It follows that

$$-(\sigma_M-1)\le \mathrm{Spec}_{E/6}\le 1-\sigma_m\quad\text{and}\quad \frac{1}{2}\le 1-\frac{\sigma_M}{4}\le \mathrm{Spec}_{Q_1}\le 1-\frac{\sigma_m}{4}.$$

Therefore,

$$\frac{1}{1/\sigma_m - 1/4} \leq \mathrm{Spec}_{Q_1^{-1}Q_2} \leq \frac{1}{1/\sigma_M - 1/4} \leq \frac{1}{1/2 - 1/4} = 4.$$

We note the estimation (Appendix 2) that

$$\sigma_m = \mathcal{O}(h^2). \tag{9}$$

Then

$$1 + \mathcal{O}(h_t) \approx 1 + \frac{Dh_t}{h^2}\frac{1}{1/\sigma_m - 1/4} \leq \mathrm{Spec}_{\boldsymbol{K}_4} \leq 1 + \frac{Dh_t}{h^2}\frac{1}{1/\sigma_M - 1/4} \leq 1 + \frac{4Dh_t}{h^2},$$

and

$$\mathrm{Spec}_{\boldsymbol{K}_4^{-1}} < 1 - \frac{Dh_t}{h^2}\frac{1}{1/\sigma_m - 1/4} \approx 1 - \mathcal{O}(h_t).$$

(2) In general, if, (i) the orbit (u, v) stays invariant in a bounded domain, and (ii) the reaction terms are in C^1 class, it follows that all the quantities

$$\|f\|_\infty, \quad \|f_u\|_\infty, \quad \|f_v\|_\infty, \quad \|g\|_\infty, \quad \|g_u\|_\infty, \quad \|g_v\|_\infty$$

are finite, and a small time step suffices. For example, choose h_t as small as to make valid the following estimate of the contraction rate

$$\begin{aligned}\|D\boldsymbol{\Phi}\| &\leq \|K_4^{-1}\|(1 + h_t(\|f_u\|_\infty + \|f_v\|_\infty)) \\ &< \|K_4^{-1}\| + \frac{(1 - \|K_4^{-1}\|)}{2} = \frac{(1 + \|K_4^{-1}\|)}{2} < 1.\end{aligned}$$

This amounts to choosing

$$h_t < \frac{(1/\|K_4^{-1}\| - 1)}{2(\|f_u\|_\infty + \|f_v\|_\infty)}.$$

We note for practical applications that the primitive variables are usually non-dimensionalised close to unity magnitude.

Up to the above analysis and notations (*overloaded* usage of $\boldsymbol{E}$), discussion of the remaining examples will be brief.

Example 3.2 (Fourth-order semi-implicit scheme)

$$\frac{3}{4}\frac{u_{P_0}^{n+1} - u_{P_0}^n}{h_t} + \frac{1}{24}\sum_{i=1}^{6}\frac{u_{P_i}^{n+1} - u_{P_i}^n}{h_t} = \frac{D}{h^2}\left(-u_{P_0}^n + \frac{1}{6}\sum_{i=1}^{6} u_{P_i}^n\right) + \frac{3}{4}f_{P_0}^n + \frac{1}{24}\sum_{i=1}^{6} f_{P_i}^n.$$

Hence

$$\begin{aligned}\boldsymbol{Q}_1 u^{n+1} &= \left(\boldsymbol{Q}_1 - \frac{Dh_t}{h^2}\boldsymbol{Q}_2\right)u^n + h_t\boldsymbol{Q}_1 f^n, \\ u^{n+1} &= \boldsymbol{A}_4 u^n + h_t f^n, \quad \text{with } \boldsymbol{A}_4 = \boldsymbol{I} - \frac{Dh_t}{h^2}\boldsymbol{Q}_1^{-1}\boldsymbol{Q}_2.\end{aligned} \tag{10}$$

(1) Pure diffusion case. In practice, the above equations are uniquely solvable at all time steps, provided that A_4 is nonsingular. We expect

$$\frac{1}{2} \le 1 - \frac{4Dh_t}{h^2} \le 1 - \frac{Dh_t}{h^2}\frac{1}{1/\sigma_M - 1/4} \le \mathrm{Spec}_{\boldsymbol{A}_4} \le 1 - \frac{Dh_t}{h^2}\frac{1}{1/\sigma_m - 1/4} \approx 1 - \mathcal{O}(h_t).$$

The left-most inequality holds in the above on the *sufficient* condition that,

$$h_t \le \frac{h^2}{8D}, \tag{11}$$

which also implies the positivity of $\boldsymbol{Q}_1 - (Dh_t/h^2)\boldsymbol{Q}_2$ in Equation (10). For any single run using h_t as just described, the iteration (also error propagation) matrix ($\boldsymbol{A}_4$) remains uniformly bounded below 1.0 in operator norm, at all time steps. The scheme is thus conditionally stable. When the spatial resolution is refined, we actually set h_t as small as proportional to (a fraction of) h^4, due to the accuracy requirement of a fourth-order method.

We refer to [18] for estimation of Laplacian eigenvalues on a *single* hexagon.

(2) With the reaction term, the *SS* procedure at each time step reads

$$\begin{aligned} u^{n+1,0} &:= u^n, \\ u^{n+1,k} &:= \boldsymbol{\Phi} u^{n+1,k-1} := \boldsymbol{A}_4 u^{n+1,k-1} + h_t f(u^n, v^n), \quad k = 1, 2, \dots . \end{aligned} \tag{12}$$

Here the functional iteration map has a constant derivative, $\boldsymbol{D\Phi} = \boldsymbol{A}_4$, and $\|\boldsymbol{D\Phi}\| = \|\boldsymbol{A}_4\|$. The convergence behaviour is identical to the case of pure diffusion.

Replacing the averaging operator ($\boldsymbol{Q}_1$) by the *identity* map in the previous two examples, we obtain the next two.

Example 3.3 (Second-order implicit scheme)

$$\frac{u_{P_0}^{n+1} - u_{P_0}^n}{h_t} = \frac{D}{h^2}\left(-u_{P_0}^{n+1} + \frac{1}{6}\sum_{i=1}^{6} u_{P_i}^{n+1}\right) + f_{P_0}^{n+1},$$

i.e.

$$\left(1 + \frac{Dh_t}{h^2}\right) u_{P_0}^{n+1} - \frac{Dh_t}{6h^2}\sum_{i=1}^{6} u_{P_i}^{n+1} = u_{P_0}^n + h_t f_{P_0}^{n+1}.$$

Therefore

$$\boldsymbol{K}_2 u^{n+1} = u^n + h_t f_{P_0}^{n+1}, \quad \text{with } \boldsymbol{K}_2 = \left(1 + \frac{Dh_t}{h^2}\right)\boldsymbol{I} - \frac{Dh_t}{6h^2}\boldsymbol{E} = \boldsymbol{I} + \frac{Dh_t}{h^2}\boldsymbol{Q}_2. \tag{13}$$

The matrix $\boldsymbol{K}_2$ is symmetric with positive diagonal entities and negative or zero off-diagonal entities, and endowed with all the qualitative properties as $\boldsymbol{K}_4$. In particular, eigenvalues of $\boldsymbol{K}_2$ and $\boldsymbol{K}_2^{-1}$ are all positive, with $\|\boldsymbol{K}_2\| > 1$ and $\|\boldsymbol{K}_2^{-1}\| < 1$. This implicit scheme is unconditionally

stable in the pure diffusion case. Similar to Example 3.1, we apply

$$\begin{aligned} u^{n+1,0} &:= u^n \\ u^{n+1,k} &:= \boldsymbol{\Phi} u^{n+1,k-1} := \boldsymbol{K}_2^{-1} u^{n+1,k-1} + h_t \boldsymbol{K}_2^{-1} f(u^{n+1,k-1}, v^{n+1,k-1}), \quad k = 1, 2, \ldots \end{aligned} \tag{14}$$

in the general case, and choose time steps to satisfy

$$\|D\boldsymbol{\Phi}\| \leq \|K_2^{-1}\|(1 + h_t(\|f_u\|_\infty + \|f_v\|_\infty)) < \frac{(1 + \|K_2^{-1}\|)}{2} < 1.$$

It is sufficient to choose

$$h_t < \frac{(1/\|K_2^{-1}\| - 1)}{2(\|f_u\|_\infty + \|f_v\|_\infty)}.$$

Here

$$1 + \mathcal{O}(h_t) \approx 1 + \frac{Dh_t}{h^2}\sigma_m \leq \mathrm{Spec}_{\boldsymbol{K}_2} \leq 1 + \frac{Dh_t}{h^2}\sigma_M \leq 1 + \frac{2Dh_t}{h^2},$$

and

$$\mathrm{Spec}_{\boldsymbol{K}_2^{-1}} \leq \frac{1}{1 + (Dh_t/h^2)\sigma_m} < 1 - \frac{Dh_t}{h^2}\sigma_m \approx 1 - \mathcal{O}(h_t).$$

Example 3.4 (Second-order explicit scheme)

$$\frac{u_{P_0}^{n+1} - u_{P_0}^n}{h_t} = \frac{D}{h^2}\left(-u_{P_0}^n + \frac{1}{6}\sum_{i=1}^{6} u_{P_i}^n\right) + f_{P_0}^n,$$

i.e.

$$u_{P_0}^{n+1} = \left(1 - \frac{Dh_t}{h^2}\right) u_{P_0}^n + \frac{Dh_t}{6h^2}\sum_{i=1}^{6} u_{P_i}^n + h_t f_{P_0}^n.$$

Then

$$u^{n+1} = \boldsymbol{A}_2 u^n + h_t f_{P_0}^n, \quad \text{with } \boldsymbol{A}_2 = \left(1 - \frac{Dh_t}{h^2}\right)\boldsymbol{I} + \frac{Dh_t}{6h^2}\boldsymbol{E} = \boldsymbol{I} - \frac{Dh_t}{h^2}\boldsymbol{Q}_2. \tag{15}$$

The iteration matrix $\boldsymbol{A}_2$ is symmetric and strictly diagonally dominant, provided that $h_t < h^2/(2D)$, which serves as the stability condition in case of pure diffusion. Indeed, choosing $h_t < h^2/(4D)$ ensures a geometric convergence rate less than 1/2. On the occurrence of reaction terms, we have a straight assignment

$$u^{n+1} := \boldsymbol{\Phi} u^n := \boldsymbol{A}_2\, u^n + h_t f(u^n, v^n). \tag{16}$$

It follows that $\boldsymbol{D\Phi} = \boldsymbol{A}_2$ and $\|\boldsymbol{D\Phi}\| = \|\boldsymbol{A}_2\|$. The stability behaviour is identical to the pure diffusion case, up to the estimate

$$1 - \frac{2Dh_t}{h^2} \leq 1 - \frac{Dh_t}{h^2}\sigma_M \leq \mathrm{Spec}_{\boldsymbol{A}_2} \leq 1 - \frac{Dh_t}{h^2}\sigma_m \approx 1 - \mathcal{O}(h_t).$$

Remark 4 There are two concerns in all the examples just discussed : solvability at a single time step and error-diminishing in the evolution. The matrices $\boldsymbol{K}_4$ and $\boldsymbol{K}_2$ being strictly diagonally dominant with any stepsize h_t, Equations (10) and (13) are numerically easily solvable. However, small h_t are chosen as analysed to make possible a contraction map, so as to diminish potential errors in the initial or boundary data and propagated (any kind) errors at intermediate steps.

This less-than-one contraction rate also contributes in the two conditionally stable examples. Our preference is the *SS* procedure, and refer to [8] for direct methods.

The schemes, Equations (6), (10) and (13), are thoroughly tested in Sections 4.3, 4.4.1, and Equations (13) and (15) in Section 4.4.2. Both smooth and non-smooth problems will be encountered.

4. Numerical experiments and discussions

4.1 *Code description*

We describe firstly our software tools developed and used in numerical experiments. Both two-level FD and method of line (MOL) methods are designed. We give some details.

(1) *Grid structure.* Cartesian type uniform grids are deployed for rectangular domains. Irregular domains are initially embedded in a cartesian grid to yield an approximation to the geometry by the procedure of Algorithm 1.
(2) *FVs.* Boundary-fitted conforming cell-centred FVM is applied. Both hexagonal type I,II, and (orthogonal) quadrilateral FVs are taken. These are denoted by *Hexa I, Hexa II* and *Quad* in Table 3, and are designed as linearly linked with no (cartesian) structure assumed. The FV type is denoted as *2D* for rectangular domains if using structured cartesian half-integral nodes.
(3) *Numerical methods.* In case of time-dependent problems, two-level Crank-Nicolson (C-N) scheme is endowed with parameter $\alpha_{\mathrm{CN}} = 0, 0.5$ or 1.0 (explicit, classical C-N, or implicit). Also designed is the MOL approach with many choices of the *integrator*. Only results of *rkf45* and *trapezoid* methods are presented.
(4) *Numerical schemes.* Standard five-point (*Q5*) and compact nine-point (*Q9c*) FD schemes are both designed using *2D* or *Quad* FVs. For *Hexa I* and *II* FVs, the options are *H7* and *H7c* schemes.
(5) *Language.* All the above are implemented in both *C* and *MATLAB*. The integration routines we adopted, in the *C* language, is from the source [11], and ode45 [17] in ©*MATLAB*.

These are summarised in Table 3.

4.2 *Validation of hexagonal grid methods on Poisson equation*

The proposed ordinary (*H7*, Equation (1)) and compact (*H7c*, Equation (4)) seven-point schemes are, in theory, exact for polynomials of degrees less than four and six, respectively. Our numerical result (not shown) justifies these are indeed second and fourth-order for monomials. Another

Table 3. Software description. All codes listed are implemented in both C and MATLAB.

Model	Structure of FVs	Temporal discretisation	Numerical method	Spatial discretisation	Applicable domain
1	2D	FD	C-N	Q5, Q9c	Cartesian
2	2D	MOL	*rkf*45, trapezoid	Q5, Q9c	Cartesian
3	Quad	FD	C-N	Q5, Q9c	Cartesian, irregular
4	Quad	MOL	*rkf*45, trapezoid	Q5, Q9c	Cartesian, irregular
5	Hexa I,II	FD	C-N	H7, H7c	Cartesian, irregular
6	Hexa I,II	MOL	*rkf*45, trapezoid	H7, H7c	Cartesian, irregular

Table 4. Accuracy in solving Poisson equation by hexagonal ordinary and compact seven-point (*H7*,*H7c*) schemes, ratio_M (ratio_2) refers to maximal (normalised 2-) norm of errors on grid. The iterative solver is Bi-CGSTAB. Both relative and absolute tolerance are 1.0e−14.

Eq.	Scheme	FVs	nx, ny	Maximal res	Maximal error	ratio_M	Two-norm error	ratio_2	Iter
A	*H7*	Hexa I	20	3.3e−13	1.6e−03		6.6e−04		56
A	*H7*	Hexa I	40	1.3e−12	3.9e−04	4.1	1.5e−04	4.4	119
A	*H7*	Hexa I	80	5.7e−12	9.5e−05	4.1	3.7e−05	4.0	226
A	*H7*	Hexa II	80	6.1e−12	2.3e−05		8.3e−06		219
A	*H7c*	Hexa I	20	2.8e−13	3.5e−06		1.8e−06		57
A	*H7c*	Hexa I	40	1.5e−12	2.2e−07	15.9	1.1e−07	16.3	114
A	*H7c*	Hexa I	80	5.5e−12	1.3e−08	16.9	6.7e−09	16.4	219
A	*H7c*	Hexa II	80	2.5e−10	3.7e−09		1.9e−09		210
G	*H7*	Hexa I	20	1.5e−11	7.2e−04		4.2e−04		64
G	*H7*	Hexa I	40	8.8e−11	1.8e−04	4.0	1.0e−04	4.2	121
G	*H7*	Hexa I	80	2.9e−10	4.4e−05	4.1	2.5e−05	4.0	230
G	*H7*	Hexa II	80	2.9e−10	2.4e−05		1.3e−05		241
G	*H7c*	Hexa I	20	1.2e−11	3.9e−08		2.4e−08		64
G	*H7c*	Hexa I	40	7.3e−11	2.5e−09	15.6	1.4e−09	17.1	120
G	*H7c*	Hexa I	80	2.6e−10	1.5e−10	16.7	8.8e−11	15.9	241
G	*H7c*	Hexa II	80	3.1e−10	6.5e−11		3.7e−11		229

two test problems were chosen, problem *A* and *G* from [12] in domain $[0,1]^2$ and $[1,2]^2$. The *Bi-CGSTAB* [15] iterative method was used in solving the discrete linear system. The result (Table 4) shows the correct order of convergence of each scheme in both the discrete maximal and normalised two-norms of errors at spatial nodes. We mention briefly that

(1) The iteration count grows linearly with respect to the mesh size in uni-direction, as expected in solving the discrete diffusion system.
(2) Computation on type II hexagonal FVs are faster and slightly more accurate than on type I, probably due to the same index (order) scheme in our design.

We note the *Bi-CGSTAB* method outperforms several other iterative methods in run-time efficiency. The Laplacian is a component of the R-D system which we discuss next. The Bi-CGSTAB method is applied in all subsequent computations.

4.3 *Validation of hexagonal grid methods on R-D system*

We solve examples of the R-D system (Equation (5)) by methods derived from Equations (6), (10) and (13). Ths following discussion refers to Table 5.

(1) *A non-homogeneous Dirichlet problem.* Here analytic solution exists

$$u(t,x,y) = \mathrm{e}^{-(2\pi^2+1)t}\sin\pi x \sin\pi y,$$
$$v(t,x,y) = \epsilon u(t,x,y).$$

The parameter values are $\epsilon = 0.01$, $D_1 = D_2 = 1.0$, and reaction terms $f(u,v) = -v/\epsilon, g(u,v) = -\epsilon u$.

(2) *A non-homogeneous Neumann problem.* The analytic solution is

$$u(t,x,y) = \mathrm{e}^{-(2\pi^2+1)t}\cos\pi x \cos\pi y,$$
$$v(t,x,y) = \epsilon\, u(t,x,y).$$

The parameters and reaction terms are identical to the previous.

Table 5. Accuracies in solving R-D systems by (i) ordinary implicit seven-point, (ii) fully and (iii) semi-implicit compact seven-point schemes. The timespan is from 0 to 0.5. Type I hexagons are used.

Problem	Scheme	n_{step}	Grid-size	itNL	max-u-err	Ratio
1	H7-implicit	500	12×10	19,469	9.260e−06	5.14
1	H7-implicit	2000	24×20	65,874	1.803e−06	1.0
1	H7-implicit	8000	48×40	240,878	4.026e−07	1.0/4.48
1	H7c-full-im	500	12×10	1000	4.248e−06	20.54
1	H7c-full-im	8000	24×20	16,000	2.068e−07	1.0
1	H7c-full-im	128,000	48×40	256,000	1.023e−08	1.0/20.22
1	H7c-semi-im	500	12×10	1000	3.473e−06	16.90
1	H7c-semi-im	8000	24×20	16,000	2.055e−07	1.0
1	H7c-semi-im	128,000	48×40	256,000	1.568e−08	1.0/13.10
2	H7-implicit	500	12×10	16,812	5.134e−05	9.65
2	H7-implicit	2000	24×20	55,182	5.321e−06	1.0
2	H7-implicit	8000	48×40	181,859	8.810e−07	1.0/6.04
2	H7c-full-im	500	12×10	5541	4.497e−05	24.29
2	H7c-full-im	8000	24×20	77,359	1.851e−06	1.0
2	H7c-full-im	128,000	48×40	1,392,010	1.417e−07	1.0/13.06
2	H7c-semi-im	500	12×10	7761	4.310e−05	24.87
2	H7c-semi-im	8000	24×20	109,615	1.733e−06	1.0
2	H7c-semi-im	128,000	48×40	1,517,042	1.391e−07	1.0/12.46

We solve these equations on approximated unit squares. Analytic solutions are used to provide the non-homogeneous Dirichlet/Neumann boundary condition on the zig-zagging global boundary. We note the BVs of primitive variables at the *ghost* cells are obtained by (only) second-order approximation using the Neumann data. This is for ease of implementation of our general-purpose code.

The simulation time is from 0.0 to $t_{end} = 0.5$. We note the following.

(1) *Algorithm.* In a two-level temporal FD methods, nonlinear fixed-point iteration (SS) is applied to solving the coupled system, Equation (5). The computation at each time step ends if two successive iterates differ less than 1.0e−13 in discrete maximal norm.
(2) *Complexity.* We denote by itNL the accumulated number of nonlinear iterations. The iteration matrix being static (constant), the *op-count* (operation count) is then proportional to $(itNL \cdot n_x \cdot n_y)$. As observed in Table 5, itNL is roughly proportional to the number of time steps, which in turn is proportional to $(n_x \cdot n_y)$ for implicit *H7* scheme, and proportional to $(n_x \cdot n_y)^2$ for both fully implicit and semi-implicit *H7c* schemes. We conclude that the *op-count* is proportional to $(n_x \cdot n_y)^2$ for the former method, and $(n_x \cdot n_y)^3$ for the latter two.
(3) *Efficiency.* As shown in the rightmost (*Ratio*) column in the table, the *H7* method is second-order accurate, while the *H7c* methods (fully implicit or semi-implicit) are (roughly) fourth-order. Accordingly, the compact schemes (*H7c*) are more cost-effective than the ordinary seven-point (*H7*) scheme, in cases of the *smooth* problems tested here.
(4) *Practical issues.* We will not comment on further possible rule(s) which might be extracted from these two particular problems, except pointing out that the restoration character of the reaction terms (endowed with negative gradients) makes the fully implicit scheme numerically better conditioned than the semi-implicit one. Finally, we note the temporal and spatial meshsizes in Table 5 satisfy the suggested constraint, Equation (11), very closely.

A non-smooth problem is considered next.

4.4 *Application to electrical wave propagation in cardiac tissue*

The cardiac electrical activity can be described with a macroscopic scale by including membrane ionic current and transmembrane potential. The resulting governing equations are the so-called bidomain equations [19], which consist of an elliptic partial differential equation and a parabolic differential equation, coupled with a system of nonlinear ordinary differential equations for ionic dynamics. As noted in [22], solving bidomain equations is computationally expensive. Under the assumption of equal anisotropies, the system of bidomain equations is reduced to monodomain equations, as an R-D system. For electrical wave propagation, differences between bidomain and monodomain equations are relatively small [10]. The system of monodomain equations is numerically efficient and accepted by many in study of electrical wave propagation of cardiac tissue [1,16,20].

In this work, we use the simple Aliev-Panfilov [1] model for ionic current activity of myocardium cell. The model, explicitly formulated below for ease of reading, is used to simulate the pulse shape and the restitution property of the canine myocardium with satisfactory precision. The monodomain equations coupled with the Aliev-Panfilov model yields

$$\begin{aligned} \frac{\partial u}{\partial t} &= \nabla(\boldsymbol{M}\nabla u) - (ku(u-a)(u-1) + uv + I_{st}), \\ \frac{\partial v}{\partial t} &= -\left(\epsilon + \mu_1 \frac{v}{u+\mu_2}\right)(v + ku(u-a-1)). \end{aligned} \tag{17}$$

Here the dimensionless variable u stands for the normalised transmembrane potential ranging from 0 to 1, and variable v describes the dynamics of slow inward current. The conductivity tensor, $\boldsymbol{M}$, is constant diagonal for the cardiac tissue we tested here, while I_{st} represents current of the stimulation. The stimulation plan (a *Heaviside* function in space) consists of a start time (1.0), the duration (10.0/12.9) and strength (-3.0). The term $ku(u-a)(u-1)$ determines the initial upstroke of the action potential of myocardium cell, and the repolarisation dynamics of the potential is properly described by the function. The parameter values are [20] $k = 8.0$, $a = 0.1$, $\epsilon = 0.01$, $\mu_1 = 0.13$ and $\mu_2 = 0.3$. Although the parameters used in the Aliev-Panfilov model do not have a specific physiological meaning but are chosen properly to reproduce some important characteristics of myocardium tissue. We mention that the matrix $\boldsymbol{M}$ can be chosen non-constant diagonal or general symmetric, depending on purpose of numerical modelling (e.g. in a computer-aided sensitivity analysis).

4.4.1 *Validation of hexagonal grid methods on monodomain equation*

Simulations are conducted by using three methods:

(1) fully implicit compact seven-point scheme, Equation (6),
(2) semi-implicit compact seven-point scheme, Equation (10), and
(3) implicit ordinary seven-point *H7* scheme, Equation (13).

Test results of these are shown in the first three blocks in Table 6. The fourth block shows result using the *H7* scheme on a doubly refined mesh. The overall average wave speeds, summarised in last row within each block in the table, suggest improvement in accuracy on the fine grid in the last two blocks using the *H7* scheme. The first two (*H7c*) schemes are more accurate than the third one, but the cost-performance (not shown) is not so great.

Table 6. Simulated wave speeds using (i) fully, (ii) semi-implicit compact seven-point and (iii) implicit ordinary seven-point schemes on evolution equations. The timespan is from 0 to 150, numbers of time steps are 22,500 or 90,000 (last block), spatial resolutions are 60×50 or 120×100 (last block).

Case	Wave	Speeds	and		Deviations
Fully-implicit compact stencil					
Average speed on j-mesh, $j = 1 \ldots 5$	1.459	1.467	1.467	1.465	1.454
One-norm deviation on j-mesh, $j = 1 \ldots 5$	0.004	0.003	0.003	0.002	0.002
Average speed on i-mesh, $i = 2 \ldots 5$		1.458	1.464	1.464	1.462
One-norm deviation on i-mesh, $i = 2 \ldots 5$		0.005	0.005	0.004	0.006
Overall average and deviation, $i, j = 2:5, 1:5$				1.462	0.005
Semi-implicit compact stencil					
Average speed on j-mesh, $j = 1 \ldots 5$	1.458	1.465	1.465	1.464	1.452
One-norm deviation on j-mesh, $j = 1 \ldots 5$	0.004	0.002	0.004	0.002	0.003
Average speed on i-mesh, $i = 2 \ldots 5$		1.458	1.460	1.463	1.462
One-norm deviation on i-mesh, $i = 2 \ldots 5$		0.005	0.006	0.004	0.006
Overall average and deviation, $i, j = 2:5, 1:5$				1.461	0.005
Implicit ordinary stencil					
Average speed on j-mesh, $j = 1 \ldots 5$	1.315	1.323	1.323	1.323	1.308
One-norm deviation on j-mesh, $j = 1 \ldots 5$	0.003	0.002	0.002	0.002	0.004
Average speed on i-mesh, $i = 2 \ldots 5$		1.317	1.318	1.319	1.320
One-norm deviation on i-mesh, $i = 2 \ldots 5$		0.006	0.007	0.003	0.007
Overall average and deviation, $i, j = 2:5, 1:5$				1.319	0.006
Implicit ordinary stencil					
Doubly refined spatial mesh					
Average speed on j-mesh, $j = 1 \ldots 5$	1.494	1.499	1.499	1.499	1.491
One-norm deviation on j-mesh, $j = 1 \ldots 5$	0.002	0.003	0.003	0.003	0.002
Average speed on i-mesh, $i = 2 \ldots 5$		1.498	1.495	1.498	1.495
One-norm deviation on i-mesh, $i = 2 \ldots 5$		0.004	0.002	0.004	0.002
Overall average and deviation, $i, j = 2:5, 1:5$				1.497	0.003

The designated stimulation plan (I_{st} in Equation (17)) of current application is far away from being C^6-smooth. We will use the ordinary seven-point methods exclusively in subsequent investigations.

4.4.2 *More tests*

To demonstrate the capability of hexagonal FVs in the study of wave phenomena, the remaining test cases consist of three categories described briefly in Table 7.

(1) *Test* 1–4. The goal is to investigate linear wave propagation (Figures 2 and 3) in cardiac tissue in an approximated square domain. Here a uni-direction linear wave started initially at the left edge of the domain, caused by electrical stimulation at the whole edge in a short time frame. The measured conduction velocities of the resulting linear waves (Tables 8–11) in these four tests are comparable with data obtained from the literature [20]. Our results indicate a trend in convergence.
(2) *Test* 5–9. Linear wave started initially as in the first category tests, it was then followed in a later time by a second stimulation at the first half of the top edge, resulting in a self-sustained spiral wave, Figure 4.
(3) *Test* 10, 11. This last category deals with computation in a reversed *C-type* domain (Figure 5), which represents a horizontal cross-section of left ventrical cardiac tissue [13].

For all test runs, computational domains consist of rectangular or hexagonal FVs. Twenty-five tracers are deployed. The calculated values of variables u and v are recorded at these tracers at various times.

Table 7. Test run description of wave phenomena using monodomain equations.

Test	Domain	t_{end}	Grid	Grid Size	Method	Code	Wave
1	Square	100	Cartesian	100×100	FD, C-N	C	Linear
2	Square	100	Cartesian	100×100	MOL,rkf45	C	Linear
3	Square	100	Hexa I	120×100	FD, C-N	C	Linear
4	Square	100	Hexa I	120×100	MOL,rkf45	C	Linear
5	Square	140	Cartesian	100×100	FD, C-N	C	Spiral
6	Square	140	Cartesian	100×100	MOL,rkf45	C	Spiral
7	Square	140	Hexa II	100×120	FD, C-N	C	Spiral
8	Square	140	Hexa I	120×100	FD, C-N	M	Spiral
9	Square	140	Hexa I	120×100	MOL,rkf45	C	Spiral
10	C-type	70	Hexa II	100×120	FD, C-N	M	Curved
11	C-type	70	Hexa II	100×120	MOL,rkf45	C	Curved

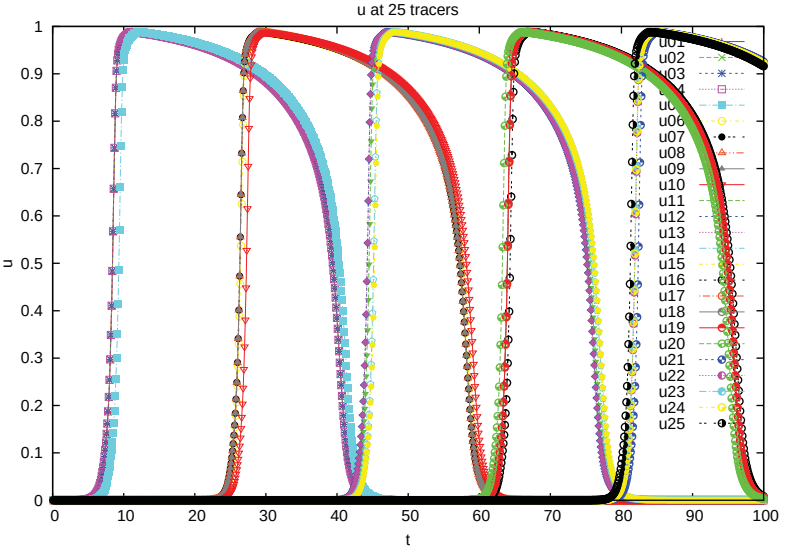

Figure 2. Linear wave recorded at 25 tracers on 50×60 type II hexagonal grid.

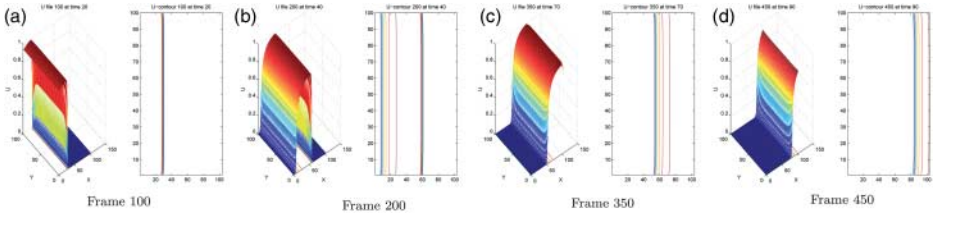

Figure 3. Linear wave on square via type I hexagons using MOL. Surface and contour plots. (a) Frame 100, (b) Frame 200, (c) Frame 350, (d) Frame 450.

4.4.3 *Results and discussion*

We discuss in more details below.

(1) *Test* 1–4. Two references, test 1 and 2, were carried out on a *120-by-120* sized square domain, with computation on standard boundary-fitted cell-centred FVs, i.e. on rectangular cartesian

Table 8. Linear wave computation by various FVs and methods. $n \approx 25$, $\Delta t = 1.0\text{e}-2$, $\Delta t/(\Delta x)^2 \approx 4.34\text{e}-4$.

Case	Model	Method	Option	FV	t_{end}	n_x, n_y	Speed	Deviation
1	1	FD	$\alpha_{\text{CN}}0.5$	2D	50	25, 25	0.718	0.0
2	1	FD	$\alpha_{\text{CN}}1.0$	2D	50	25, 25	0.720	0.0
3	1	FD	$\alpha_{\text{CN}}0.0$	2D	50	25, 25	0.716	0.0
4, 5	2	MOL	Trapezoid, rkf45	2D	50	25, 25	0.718	0.0
6	3	FD	$\alpha_{\text{CN}}0.5$	Quad	50	25, 25	0.718	0.0
7	3	FD	$\alpha_{\text{CN}}1.0$	Quad	50	25, 25	0.720	0.0
8	3	FD	$\alpha_{\text{CN}}0.0$	Quad	50	25, 25	0.716	0.0
9,10	4	MOL	Trapezoid, rkf45	Quad	50	25, 25	0.718	0.0
11	5	FD	$\alpha_{\text{CN}}0.5$	Hexa II	50	25, 30	0.770	0.018
12	5	FD	$\alpha_{\text{CN}}1.0$	Hexa II	50	25, 30	0.773	0.018
13	5	FD	$\alpha_{\text{CN}}0.0$	Hexa II	50	25, 30	0.766	0.018
14,15	6	MOL	Trapezoid, rkf45	Hexa II	50	25, 30	0.770	0.018
16	5	FD	$\alpha_{\text{CN}}0.5$	Hexa I	50	30, 25	1.018	0.021
17	5	FD	$\alpha_{\text{CN}}1.0$	Hexa I	50	30, 25	1.022	0.021
18	5	FD	$\alpha_{\text{CN}}0.0$	Hexa I	50	30, 25	1.013	0.021
19,20	6	MOL	Trapezoid, rkf45	Hexa I	50	30, 25	1.018	0.021

Table 9. Linear wave computation by various FVs and methods. $n \approx 50$, $\Delta t = 2.5\text{e}-3$, $\Delta t/(\Delta x)^2 \approx 4.34\text{e}-4$.

Case	Model	Method	Option	FV	t_{end}	n_x, n_y	Speed	Deviation
1	1	FD	$\alpha_{\text{CN}}0.5$	2D	50	50, 50	1.240	0.003
2	1	FD	$\alpha_{\text{CN}}1.0$	2D	50	50, 50	1.248	0.002
3	1	FD	$\alpha_{\text{CN}}0.0$	2D	50	50, 50	1.234	0.002
4, 5	2	MOL	Trapezoid, rkf45	2D	50	50, 50	1.240	0.003
6	3	FD	$\alpha_{\text{CN}}0.5$	Quad	50	50, 50	1.240	0.004
7	3	FD	$\alpha_{\text{CN}}1.0$	Quad	50	50, 50	1.248	0.002
8	3	FD	$\alpha_{\text{CN}}0.0$	Quad	50	50, 50	1.233	0.002
9,10	4	MOL	Trapezoid, rkf45	Quad	50	50, 50	1.240	0.004
11	5	FD	$\alpha_{\text{CN}}0.5$	Hexa II	50	50, 60	1.238	0.006
12	5	FD	$\alpha_{\text{CN}}1.0$	Hexa II	50	50, 60	1.247	0.006
13	5	FD	$\alpha_{\text{CN}}0.0$	Hexa II	50	50, 60	1.231	0.005
14,15	6	MOL	Trapezoid, rkf45	Hexa II	50	50, 60	1.238	0.006
16	5	FD	$\alpha_{\text{CN}}0.5$	Hexa I	50	60, 50	1.364	0.010
17	5	FD	$\alpha_{\text{CN}}1.0$	Hexa I	50	60, 50	1.373	0.010
18	5	FD	$\alpha_{\text{CN}}0.0$	Hexa I	50	60, 50	1.356	0.009
19,20	6	MOL	Trapezoid, rkf45	Hexa I	50	60, 50	1.364	0.010

(half-integral) nodes. These are FD codes using either C-N method (test 1) or MOL by rkf45 (test 2).

Test 3 (4) is using type I hexagonal FVs approximating the square domain, with computation done by FD (MOL) method. Time plots of the dependent variables at twenty-five tracers are shown in Figure 2. Visualisation by *MATLAB* of test 4 is seen as Figure 3. These figures indicate clearly a linear wave solution. Plots of tests 1–3 are similar and omitted.

More were examined to validate our methods and implementations. The wave speeds are calculated at (up to) 25 tracers by backward Euler scheme in time as listed in Tables 8–11, in which gradually finer spatial resolutions are taken. The average conduction velocities (measured at relevant tracers) and their deviations are recorded. The simulations were conducted based on four different temporial-spatial discretisations. The first two models (test 1,2) were thought to be more robust. To our surprise, the *Hexa II* results are compatible to the results on rectangular and general *Quad* FVs, while the *Hexa I* results converge even faster than all

Table 10. Linear wave computation by various FVs and methods. $n \approx 100$, $\Delta t = 2.5\text{e}-3$, $\Delta t/(\Delta x)^2 \approx 1.736\text{e}-3$.

Case	Model	Method	Option	FV	t_{end}	n_x, n_y	Speed	Deviation
1	1	FD	$\alpha_{\text{CN}}0.5$	2D	150	100,100	1.461	0.003
2	1	FD	$\alpha_{\text{CN}}1.0$	2D	150	100,100	1.472	0.014
3	1	FD	$\alpha_{\text{CN}}0.0$	2D	150	100,100	1.461	0.003
4	2	MOL	Trapezoid	2D	150	100,100	1.461	0.003
5	2	MOL	rkf45	2D	150	100,100	1.462	0.003
6	3	FD	$\alpha_{\text{CN}}0.5$	Quad	150	100,100	1.462	0.003
7	3	FD	$\alpha_{\text{CN}}1.0$	Quad	150	100,100	1.464	0.001
8	3	FD	$\alpha_{\text{CN}}0.0$	Quad	150	100,100	1.459	0.005
9,10	4	MOL	Trapezoid, rkf45	Quad	150	100,100	1.462	0.003
11	5	FD	$\alpha_{\text{CN}}0.5$	Hexa II	150	100,120	1.463	0.004
12	5	FD	$\alpha_{\text{CN}}1.0$	Hexa II	150	100,120	1.466	0.002
13	5	FD	$\alpha_{\text{CN}}0.0$	Hexa II	150	100,120	1.461	0.004
14,15	6	MOL	Trapezoid, rkf45	Hexa II	150	100,120	1.463	0.004
16	5	FD	$\alpha_{\text{CN}}0.5$	Hexa I	150	120,100	1.521	0.011
17	5	FD	$\alpha_{\text{CN}}1.0$	Hexa I	150	120,100	1.525	0.010
18	5	FD	$\alpha_{\text{CN}}0.0$	Hexa I	150	120,100	1.519	0.011
19	6	MOL	Trapezoid	Hexa I	150	120,100	1.522	0.011
20	6	MOL	rkf45	Hexa I	150	120,100	1.521	0.011

Table 11. Linear wave computation by various FVs and methods. $n \approx 200$ or 400, $\Delta t = 6.25\text{e}-4$, or $1.5625\text{e}-4$, ratio $\Delta t/(\Delta x)^2 \approx 1.736\text{e}-3$ for all cases.

Case	Model	Method	Option	FV	t_{end}	n_x, n_y	Speed	Deviation
1	1	FD	$\alpha_{\text{CN}}0.5$	2D	150	200,200	1.555	0.001
2	1	FD	$\alpha_{\text{CN}}1.0$	2D	150	200,200	1.556	0.001
3	1	FD	$\alpha_{\text{CN}}0.0$	2D	150	200,200	1.554	0.001
4, 5	2	MOL	Trapezoid, rkf45	2D	150	200,200	1.555	0.001
6	3	FD	$\alpha_{\text{CN}}0.5$	Quad	150	200,200	1.555	0.001
7	3	FD	$\alpha_{\text{CN}}1.0$	Quad	150	200,200	1.556	0.000
8	3	FD	$\alpha_{\text{CN}}0.0$	Quad	150	200,200	1.554	0.002
9,10	4	MOL	Trapezoid, rkf45	Quad	150	200,200	1.555	0.001
11	5	FD	$\alpha_{\text{CN}}0.5$	Hexa II	150	200,240	1.555	0.001
12	5	FD	$\alpha_{\text{CN}}1.0$	Hexa II	150	200,240	1.555	0.001
13	5	FD	$\alpha_{\text{CN}}0.0$	Hexa II	150	200,240	1.554	0.001
14,15	6	MOL	Trapezoid, rkf45	Hexa II	150	200,240	1.555	0.001
16	5	FD	$\alpha_{\text{CN}}0.5$	Hexa I	150	240,200	1.578	0.014
17	5	FD	$\alpha_{\text{CN}}1.0$	Hexa I	150	240,200	1.579	0.015
18	5	FD	$\alpha_{\text{CN}}0.0$	Hexa I	150	240,200	1.577	0.014
19,20	6	MOL	Trapezoid, rkf45	Hexa I	150	240,200	1.578	0.014
21	1	FD	$\alpha_{\text{CN}}0.0$	2D	100	400,400	1.580	0.000
22	3	FD	$\alpha_{\text{CN}}0.0$	Quad	100	400,400	1.580	0.000
23	5	FD	$\alpha_{\text{CN}}0.0$	Hexa II	100	400,480	1.580	0.001
24	5	FD	$\alpha_{\text{CN}}0.0$	Hexa I	100	480,400	1.595	0.018

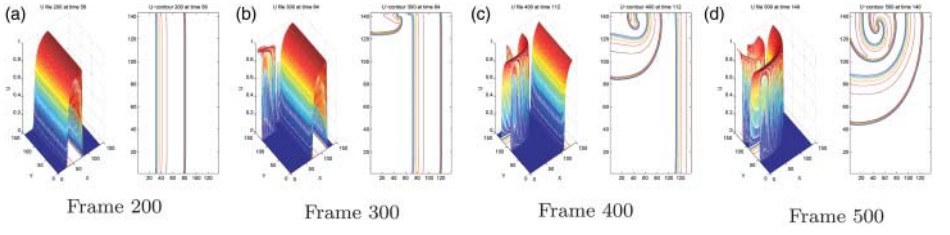

Figure 4. Spiral wave on square via type II hexagons using FD. Surface and contour plots. (a) Frame 200, (b) Frame 300, (c) Frame 400, (d) Frame 500.

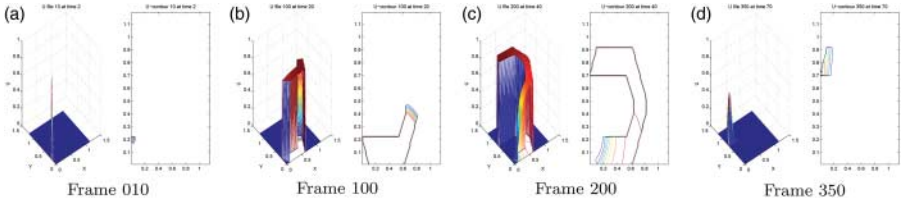

Figure 5. Linear wave on curved domain via type II hexagons using MOL. Surface and contour plots. (a) Frame 010, (b) Frame 100, (c) Frame 200, (d) Frame 350.

other tested methods, including those based on structured cartesian (*2D*) grids. The authors make a strong point that

hexagonal FVs are valuable in simulations of two-dimensional wave phenomena.

(2) *Test* 5–9. These are simulations of spiral waves with some results shown in Figure 4, for test 7. The simulation time is up to *140* for all computations.

Test 5 is a reference case for spiral wave on the square domain, deployed with 100-by-100 rectangular FV nodes. FD method in a Crank–Nicolson variation is applied. Another reference is test 6 by MOL. The surface and contour plots of these two referential cases are in good agreement, but not shown because of limitation of space. Test 7 runs on *100-by-120* type II hexagons by FD, with result in Figure 4, showing a self-sustained spiral wave. This and the previous two rectangular grid tests produced quite similar patterns in all phases, indicating the capability of hexagonal FVs in numerical modelling.

Tests 8 and 9 run on *120-by-100* type I hexagons by FD and M-code (test 8) or MOL and C-code (test 9). The plots of these two tests are also in very good agreement.

(3) *Test* 10, 11. A (reversed) C-type domain is taken here. Type II hexagons are adopted as is in test 7. The grid sizes on the background are the same. The calculated results are thus conceivable. The programs are written in *MATLAB* via *C-N* scheme for test 10, and in *C*-language via *rkf45* for test 11. Calculated results of these two successfully show a travelling wave through the curved domain. The figures show very similar evolutions, thus validating our implementations and the findings. Evolution of the wave and shape of the curved domain is shown in Figure 5 for test 11.

We mention that for the horizontal section of the left ventricle case, we can introduce the fibre anisotropy effect; that is, the fibre direction is tangent to the circumferential shells of every transmural layer (endocardium, mid-myocardium, epicardium) (see [6]) and the conduction velocity is faster along this tangent direction which can be implemented by adjusting the diffusion coefficients matrix for further studies.

5. Conclusions

In this work, we develop an FV-based FD approach to solving Laplacian-related differential equations on regular hexagonal grids with a general phase angle. Explicit leading error term in the error estimation are derived. Both ordinary and compact hexagonal seven-point schemes are investigated. Theoretical properties of the associated linear (linearised) algebraic systems in solving static (time-dependent) problems are determined. Fundamental algorithm for construction of linearly linked hexagonal FVs are formulated and used to design MOL-FD and FD-FD simulation software, which can solve systems of differential equations involving general geometry by embedding into a cartesian grid.

Test results on static Poisson problems and smooth R-D systems confirm all theoretical predictions. Additionally, we apply the method to solve a system of equations on a two-dimensional cardiac tissue. The dynamics of electrical wave propagation are observed. Both linear and spiral waves are exhibited on a square-like domain using a variant of the monodomain equations. Also successfully demonstrated is a linear wave propagation in a reversed C-type domain. All computational methods and results are thoroughly and carefully examined.

The hexagonal FV approach is of great value in application to numerical heart modelling. We think this holds true for a variety of applications in two-dimensional irregular domains.

Acknowledgements

The authors are grateful to Tunghai University, Providence University, Taichung Veterans General Hospital, and the National Science Council for continued laboratory support for a long period of time, partially under the grants NSC96-2115M126002 and TCVGH-PU968109.

References

[1] R.R. Aliev and A.V. Panfilov, *A simple two-variables model of cardiac excitation*, Chaos, Solitons Fractals 7(3) (1996), pp. 293–301.
[2] F.L. Bauer and C.T. Fike, *Norms and exclusion theorems*, Numer. Math. 2 (1960), pp. 137–141.
[3] A. Berman and R.J. Plemmons, *Nonnegative Matrices in the Mathematical Sciences*, SIAM, Philadelphia, PA, 1994.
[4] B. He, *Modeling and Imaging of Bio-electrical Activity: Principle and Applications*, Kluwer Academic/Plenum Publishers, New York, 2004.
[5] S. Karaa and J. Zhang, *Analysis of stationary iterative methods for the discrete convection-diffusion equation with a 9-point compact scheme*, J. Comp. Appl. Math. 154 (2003), pp. 447–476.
[6] I.J. LeGrice, B.H. Smaill, L.Z. Chai, S.G. Edgar, J.B. Gavin, and P.J. Hunter, *Laminar structure of the heart: Ventricular myocyte arrangement and connective tissue architecture in the dog*, Am. J. Physiol. 269(2) Pt 2 (1995), pp. H571–82.
[7] M. Lorange and R.M. Gulrajani, *A computer heart model incorporating anisotropic propagation. I. Model construction and simulation of normal activation*, J Electrocardiol. 26(4) (1993), pp. 245–261.
[8] G. Meurant, *A review on the inverse of symmetric tridiagonal and block tridiagonal matrices*, SIAM J. Matrix Anal. Appl. 13(3) (1992), pp. 707–728.
[9] W.M. Pickering, *On the solution of Poisson's equation on a regular hexagonal grid using FFT methods*, JCP 64 (1986), pp. 320–333.
[10] M. Postse, B. Dube, J. Richer, A. Vinet, and R.M. Gulrajani, *A comparison of monodomain and bidomain reaction-diffusion models for action potential propagation in the human heart*, IEEE Trans. Biomed. Eng. 53(12) (2006), pp. 2425–2435.
[11] W.H. Press, S.A. Teukolsky, W.T. Vetterling, and B.P. Flannery, *Numerical Recipes in C, the Art of Scientific Computing*, 2nd ed., Cambridge University Press, New York, NY, 2002.
[12] J.R. Rice and R.F. Boisvert, *Solving Elliptic Problems with ELLPACK*, Springer-Verlag, New York, NY, 1985.
[13] H.J. Ritsema van Eck, J.A. Kors, and G. van Herpen, *The U wave in the electrocardiogram: A solution for a 100-year-old riddle*, Cardiovasc Res. 67(2) (2005), pp. 256–262.
[14] J.B. Roser, *Nine point difference solutions for Poisson's equation*, Comp. Math. Appl. 1 (1975), pp. 351–360.
[15] Y. Saad, *Iterative Methods for Sparse Linear System*, 2nd ed., SIAM, Philadelphia, PA, 2003.
[16] H. Sakaguchi and T. Fujimoto, *Elimination of spiral chaos by periodic force for the Aliev-Panfilov model*, Phys. Rev. E 71 (2005), p. 052901.
[17] L.F. Shampine, I. Gladwell, and S. Thompson, *Solving ODEs with MATLAB*, Cambridge University Press, New York, NY, 2003.
[18] Jia-chang Sun, *On approximation of Laplacian eigenproblem over a regular hexagon with zero boundary condition*, J. Clin. Microbiol. 22(2) (2004), pp. 275–286.
[19] L. Tung, *A bi-domain model for describing ischemic myocardial D-C potentials*, Ph.D. diss., MIT, Cambridge, MA, 1978.
[20] K.H.W.J. ten Tusscher and A.V. Panfilov, *Wave propagation in excitable media with randomly distributed obstacles*, Multiscale Model Simul. 3(2) (2005), pp. 265–282.
[21] H.K. Versteeg and W. Malalasekera, *An Introduction to Computational Fluid Dynamics, the Finite Volume Method*, Longman Group Ltd, New York, NY, 1995.
[22] E.J. Vigmond, R.W.d. Santos, A.J. Prassl, M. Deocw, and G. Plank, *Solvers for the cardiac bidomain equations*, Prog. Biophys. Mol. Biol. 96 (2008), pp. 3–18.

Appendix 1. Hexagon related trigonometric identities

To complete the proof of Theorem 2.1 for a hexagon with phase angle φ, we note firstly

LEMMA A.1

$$\sum_{j=1}^{6}\cos(k\theta_j)=\sum_{j=1}^{6}\sin(k\theta_j)=0,\quad 1\le k\le 5,$$

$$\frac{1}{6}\sum_{j=1}^{6}\cos(6\theta_j)=\cos(6\varphi),\quad \frac{1}{6}\sum_{j=1}^{6}\sin(6\theta_j)=\sin(6\varphi).$$

Proof Note

$$\sum_{j=1}^{6}\mathrm{e}^{\mathrm{i}k\theta_j}=\mathrm{e}^{\mathrm{i}k\varphi}\sum_{j=1}^{6}\mathrm{e}^{\mathrm{i}(kj\pi/3)}=\mathrm{e}^{\mathrm{i}k\varphi}\frac{\mathrm{e}^{\mathrm{i}(k\pi/3)}(1-\mathrm{e}^{\mathrm{i}(6k\pi/3)})}{1-\mathrm{e}^{\mathrm{i}(k\pi/3)}}=0,\quad 1\le k\le 5.$$

The case $k=6$ is readily proved in the first part of the above identity. ■

The next two lemmas are used in proving Theorem 2.1.

LEMMA A.2

$$\frac{1}{6}\sum_{j=1}^{6}\cos^k(\theta_j)=\frac{1}{6}\sum_{j=1}^{6}\sin^k(\theta_j)=\begin{cases}0, & k=1,3,5,\\ \frac{1}{2}, & k=2,\\ \frac{3}{8}, & k=4,\end{cases}$$

and

$$\frac{1}{6}\sum_{j=1}^{6}\cos^6\theta_j=\frac{1}{32}(10+\cos(6\varphi)),\quad \frac{1}{6}\sum_{j=1}^{6}\sin^6\theta_j=\frac{1}{32}(10-\cos(6\varphi)).$$

Proof These are valid by Lemma A.1 and the following trigonometric identities:

$$\cos^2\theta=\tfrac{1}{2}(1+\cos 2\theta),\qquad \sin^2\theta=\tfrac{1}{2}(1-\cos 2\theta),$$
$$\cos^3\theta=\tfrac{1}{4}(3\cos\theta+\cos 3\theta),\qquad \sin^3\theta=\tfrac{1}{4}(3\sin\theta-\sin 3\theta),$$
$$\cos^4\theta=\tfrac{1}{8}(3+4\cos 2\theta+\cos 4\theta),\qquad \sin^4\theta=\tfrac{1}{8}(3-4\cos 2\theta+\cos 4\theta),$$
$$\cos^5\theta=\tfrac{1}{16}(10\cos\theta+5\cos 3\theta+\cos 5\theta),\qquad \sin^5\theta=\tfrac{1}{16}(10\sin\theta-5\sin 3\theta+\cos 5\theta),$$
$$\cos^6\theta=\tfrac{1}{32}(10+15\cos 2\theta+6\cos 4\theta+\cos 6\theta),\qquad \sin^6\theta=\tfrac{1}{32}(10-15\cos 2\theta+6\cos 4\theta-\cos 6\theta).$$

■

LEMMA A.3 $N=n+m, 1\le n\le N-1$,

$$N=1,3,5,\ldots\qquad \frac{1}{6}\sum_{j=1}^{6}\sin^n\theta_j\cos^m\theta_j=0.$$

$$N=2, n=1, m=1,\qquad \frac{1}{6}\sum_{j=1}^{6}\sin^1\theta_j\cos^1\theta_j=0.$$

$$N=4, n=1, m=3,\qquad \frac{1}{6}\sum_{j=1}^{6}\sin^1\theta_j\cos^3\theta_j=0.$$

$$N=4, n=3, m=1, \qquad \frac{1}{6}\sum_{j=1}^{6}\sin^3\theta_j\cos^1\theta_j = 0.$$

$$N=4, n=2, m=2, \qquad \frac{1}{6}\sum_{j=1}^{6}\sin^2\theta_j\cos^2\theta_j = \frac{1}{8}.$$

$$N=6, n=1, m=5, \qquad \frac{1}{6}\sum_{j=1}^{6}\sin^1\theta_j\cos^5\theta_j = \frac{1}{32}\sin(6\varphi).$$

$$N=6, n=5, m=1, \qquad \frac{1}{6}\sum_{j=1}^{6}\sin^5\theta_j\cos^1\theta_j = \frac{1}{32}\sin(6\varphi).$$

$$N=6, n=2, m=4, \qquad \frac{1}{6}\sum_{j=1}^{6}\sin^2\theta_j\cos^4\theta_j = \frac{1}{32}(2-\cos 6\varphi).$$

$$N=6, n=4, m=2, \qquad \frac{1}{6}\sum_{j=1}^{6}\sin^4\theta_j\cos^2\theta_j = \frac{1}{32}(2+\cos 6\varphi).$$

$$N=6, n=3, m=3, \qquad \frac{1}{6}\sum_{j=1}^{6}\sin^3\theta_j\cos^3\theta_j = -\frac{1}{32}\sin(6\varphi).$$

Proof The neighbour nodes P_j's, $1 \le j \le 6$, are invariant under reflection with respect to the central node P_0. With indices periodically extended, we obtain, for odd N,

$$\sum_{j=1}^{6}\sin^n\theta_j\cos^m\theta_j = \sum_{j=1}^{6}\sin^n\theta_{j+3}\cos^m\theta_{j+3} = \sum_{j=1}^{6}\sin^n(\pi+\theta_j)\cos^m(\pi+\theta_j)$$

$$= (-1)^{n+m}\sum_{j=1}^{6}\sin^n\theta_j\cos^m\theta_j = 0.$$

The remaining cases follow from Lemma A.1 and the following identities:

$$\sin^1\theta\cos^1\theta = \tfrac{1}{2}\sin 2\theta, \qquad \sin^3\theta\cos^3\theta = \tfrac{1}{32}(3\sin 2\theta - \sin 6\theta).$$

$$\sin^2\theta\cos^2\theta = \tfrac{1}{8}(1-\cos 4\theta), \qquad \sin^1\theta\cos^5\theta = \tfrac{1}{32}(5\sin 2\theta + 4\sin 4\theta + \sin 6\theta),$$

$$\sin^1\theta\cos^3\theta = \tfrac{1}{8}(2\sin 2\theta + \sin 4\theta), \qquad \sin^5\theta\cos^1\theta = \tfrac{1}{32}(5\sin 2\theta - 4\sin 4\theta + \sin 6\theta),$$

$$\sin^3\theta\cos^1\theta = \tfrac{1}{8}(2\sin 2\theta - \sin 4\theta), \qquad \sin^2\theta\cos^4\theta = \tfrac{1}{32}(2+\cos 2\theta - 2\cos 4\theta - \cos 6\theta),$$

$$\sin^4\theta\cos^2\theta = \tfrac{1}{32}(2-\cos 2\theta - 2\cos 4\theta + \cos 6\theta),$$

These are easily verified, with appropriate choices of α in the substitutions $\sin\alpha = (e^{i\alpha} - e^{-i\alpha})/(2i)$ and $\cos\alpha = (e^{i\alpha} + e^{-i\alpha})/2$. This proves the lemma and Theorem 2.1. ■

We remark that the proof of Theorem 2.1 is largely reduced for special cases with $\varphi = 0, -\pi/6$ in the presence of some symmetries.

Appendix 2. Lower eigen value bound of hex-seven-point Laplacian

We prove the assertion, Equation (9), for a geometric discretisation which consists of (subset of) a cartesian mesh of regular hexagons. For comparison, we consider a uniform FD grid of size $(n_x+1)\cdot(n_y+1)$ on the unit square. Interior nodes are indexed by column, i.e. index $:= j + (i-1)n_y$, $1 \le i \le n_x$, $1 \le j \le n_y$. The re-scaled discrete (negative) five-point Laplacian with homogeneous Dirichlet boundary condition is represented by a *block-tridiagonal* matrix, $\boldsymbol{Lap}_5 = \mathrm{trid}(-\boldsymbol{I}, 4\boldsymbol{I}-\boldsymbol{T}, -\boldsymbol{I})$, in terms of the symmetric bi-shift operator $\boldsymbol{T} := \boldsymbol{S}^T + \boldsymbol{S} := \mathrm{trid}(1,0,1)$, and the (forward) shift $\boldsymbol{S} := \mathrm{trid}(0,0,1)$. Here the block size is n_y-by-n_y.

$$
\boldsymbol{Lap}_7 = \begin{bmatrix}
\begin{pmatrix} 6 & -1 & 0 & 0 & 0 \\ -1 & 6 & -1 & 0 & 0 \\ 0 & -1 & 6 & -1 & 0 \\ 0 & 0 & -1 & 6 & -1 \\ 0 & 0 & 0 & -1 & 6 \end{pmatrix} & \begin{pmatrix} -1 & 0 & 0 & 0 & 0 \\ -1 & -1 & 0 & 0 & 0 \\ 0 & -1 & -1 & 0 & 0 \\ 0 & 0 & -1 & -1 & 0 \\ 0 & 0 & 0 & -1 & -1 \end{pmatrix} & & & & & & & & & \\
\begin{pmatrix} -1 & -1 & 0 & 0 & 0 \\ 0 & -1 & -1 & 0 & 0 \\ 0 & 0 & -1 & -1 & 0 \\ 0 & 0 & 0 & -1 & -1 \\ 0 & 0 & 0 & 0 & -1 \end{pmatrix} & \begin{pmatrix} 6 & -1 & 0 & 0 & 0 \\ -1 & 6 & -1 & 0 & 0 \\ 0 & -1 & 6 & -1 & 0 \\ 0 & 0 & -1 & 6 & -1 \\ 0 & 0 & 0 & -1 & 6 \end{pmatrix} & \begin{pmatrix} -1 & -1 & 0 & 0 & 0 \\ 0 & -1 & -1 & 0 & 0 \\ 0 & 0 & -1 & -1 & 0 \\ 0 & 0 & 0 & -1 & -1 \\ 0 & 0 & 0 & 0 & -1 \end{pmatrix} & & & & & & & \\
 & & \begin{pmatrix} -1 & 0 & 0 & 0 & 0 \\ -1 & -1 & 0 & 0 & 0 \\ 0 & -1 & -1 & 0 & 0 \\ 0 & 0 & -1 & -1 & 0 \\ 0 & 0 & 0 & -1 & -1 \end{pmatrix} & \begin{pmatrix} 6 & -1 & 0 & 0 & 0 \\ -1 & 6 & -1 & 0 & 0 \\ 0 & -1 & 6 & -1 & 0 \\ 0 & 0 & -1 & 6 & -1 \\ 0 & 0 & 0 & -1 & 6 \end{pmatrix} & \begin{pmatrix} -1 & 0 & 0 & 0 & 0 \\ -1 & -1 & 0 & 0 & 0 \\ 0 & -1 & -1 & 0 & 0 \\ 0 & 0 & -1 & -1 & 0 \\ 0 & 0 & 0 & -1 & -1 \end{pmatrix} & & & & & \\
 & & & \begin{pmatrix} -1 & -1 & 0 & 0 & 0 \\ 0 & -1 & -1 & 0 & 0 \\ 0 & 0 & -1 & -1 & 0 \\ 0 & 0 & 0 & -1 & -1 \\ 0 & 0 & 0 & 0 & -1 \end{pmatrix} & \begin{pmatrix} 6 & -1 & 0 & 0 & 0 \\ -1 & 6 & -1 & 0 & 0 \\ 0 & -1 & 6 & -1 & 0 \\ 0 & 0 & -1 & 6 & -1 \\ 0 & 0 & 0 & -1 & 6 \end{pmatrix} & \begin{pmatrix} -1 & -1 & 0 & 0 & 0 \\ 0 & -1 & -1 & 0 & 0 \\ 0 & 0 & -1 & -1 & 0 \\ 0 & 0 & 0 & -1 & -1 \\ 0 & 0 & 0 & 0 & -1 \end{pmatrix} & & & \\
 & & & & \begin{pmatrix} -1 & 0 & 0 & 0 & 0 \\ -1 & -1 & 0 & 0 & 0 \\ 0 & -1 & -1 & 0 & 0 \\ 0 & 0 & -1 & -1 & 0 \\ 0 & 0 & 0 & -1 & -1 \end{pmatrix} & \begin{pmatrix} 6 & -1 & 0 & 0 & 0 \\ -1 & 6 & -1 & 0 & 0 \\ 0 & -1 & 6 & -1 & 0 \\ 0 & 0 & -1 & 6 & -1 \\ 0 & 0 & 0 & -1 & 6 \end{pmatrix}
\end{bmatrix}
$$

The matrix representation of re-scaled discrete seven-point Laplacian, on an indexed-by-column cartesian grid of type I hexagons (Figure 1(a) without colour labels), reads (with $n_x = n_y = 5$)
That is

$$\boldsymbol{Lap}_7 = \text{trid}(-\boldsymbol{I} - \boldsymbol{P},\ 6\boldsymbol{I} - \boldsymbol{T},\ -\boldsymbol{I} - \boldsymbol{P}^T) \equiv 2\boldsymbol{I} + \boldsymbol{Lap}_5 + \mathcal{P}, \tag{A1}$$

with *perturbation* $\mathcal{P} := \text{diag}(-\boldsymbol{P}, \boldsymbol{0}, -\boldsymbol{P}^T)$, where $\boldsymbol{P} := \boldsymbol{S}$, or $\boldsymbol{S}^T$ alternatingly between odd- and even-row blocks. Therefore the Bauer-Fike [2] theorem, applied to the diagonalizable matrix $\boldsymbol{Lap}_5$, yields

$$\max_{\sigma \in \text{Spec}_{\boldsymbol{Lap}_7}} \min_{\mu \in \text{Spec}_{2\boldsymbol{I}+\boldsymbol{Lap}_5}} \{|\sigma - \mu|\} \le \|\mathcal{P}\|_\infty = 2, \tag{A2}$$

which, together with the fact that,

$$\text{Spec}_{\boldsymbol{Lap}_5} = \left\{ 4 - 2\cos\left(\frac{p\pi}{n_x+1}\right) - 2\cos\left(\frac{q\pi}{n_y+1}\right) \middle| 1 \le p \le n_x, 1 \le q \le n_y \right\},$$

implies

$$\mathcal{O}((n_x+1)^{-2} + (n_y+1)^{-2}) \approx 4 - 2\cos\left(\frac{\pi}{n_x+1}\right) - 2\cos\left(\frac{\pi}{n_y+1}\right) = \min \text{Spec}_{Lap_5} \le \min \text{Spec}_{Lap_7}.$$

It is obvious this argument (Equations (A1) and (A2)) is valid, at matrix level, with various permuted $\mathcal{P}$ in many general situations. Finally, we note for a type I hexagon cartesian mesh approximating the unit square, we choose $h = 1/(\sqrt{3}n_x + \sqrt{3}^{-1})$, and $h = 1/(2n_x)$ for a type II mesh. Thus proves the assertion.

Remark A.1 The argument and notation ($\boldsymbol{Lap}_5$) above was simplified by having assumed the usual FD *integral* nodes for convenience. Actually, cell-centre FV approach is taken in all our work.

As such, in case of homogeneous Dirichlet B.C. on the square domain, boundary values (at centres of ghost cells) are set *via* second-order interpolation as negations of the adjacent interior values. To eliminate optionally the dependence on the BVs, we can shift the loads to weights on diagonal entities of the matrix, instead of moving BVs to the right-hand side of the linear system. Consequently, several 4's on the diagonal of the five-point Laplacian are increased to 5 or 6, and increasing from 6's to 7, 8, 9 or 10 for the hex-seven-point Laplacian, depending on the connectivities at interior nodes to ghost cells.

However, such changes on the diagonal only make slightly larger the upper bound estimate of eigen values, i.e. $\sigma_M = 2$ achieved in Equation (8) while preserving the same eigen basis. Actually, in this setup with slightly more weighted diagonal,

$$\text{Spec}_{\boldsymbol{Lap}_5} = \left\{ 4 - 2\cos\left(\frac{p\pi}{n_x}\right) - 2\cos\left(\frac{q\pi}{n_y}\right) \middle| 1 \le p \le n_x, 1 \le q \le n_y \right\},$$

with associated eigen basis

$$U^{p,q} := \left(U^{p,q}_{i,j} = \sin\left(\frac{(i-0.5)p\pi}{n_x}\right) \cdot \sin\left(\frac{(j-0.5)q\pi}{n_y}\right) \right)_{\substack{i=1:n_x,\\ j=1:n_y.}}, \quad 1 \le p \le n_x,\ \ 1 \le q \le n_y.$$

The (asymptotic) lower bound estimates are still valid.

We note the homogeneous Neumann and some Robin cases can be analysed similarly at matrix level. For example, the eigen system of homogeneous Neumann problem (at half-integral nodes) are solved by *complete* eigen pairs,

$$\lambda_{p,q} = 4 - 2\cos\left(\frac{(p-1)\pi}{n_x}\right) - 2\cos\left(\frac{(q-1)\pi}{n_y}\right),$$
$$U^{p,q}_{i,j} = \cos\left(\frac{(i-0.5)\cdot(p-1)\pi}{n_x}\right) \cdot \cos\left(\frac{(j-0.5)\cdot(q-1)\pi}{n_y}\right),$$

with $1 \le p \le n_x, 1 \le q \le n_y$.

We will not go into details in the design of operations on the zigzagging boundary cells at the *algorithms and data structures* level.